

Continuum Mechanics and Thermodynamics manuscript No.  
 (will be inserted by the editor)

## Self-gravitating Stellar Systems and Non-extensive Thermodynamics

Masaaki Sakagami<sup>1</sup>, Atsushi Taruya<sup>2</sup>

<sup>1</sup> Graduate School of Human and Environmental Studies, Kyoto University, Kyoto 606-8501, Japan

<sup>2</sup> Research Center for the Early Universe (RESCUE), School of Science, University of Tokyo, Tokyo 113-0033, Japan

Received: date / Accepted: date

**A bstract.** After introducing fundamental properties of the self-gravitating systems, we present an application of Tsallis' generalized entropy to analysis for their thermodynamical nature. Extremizing the Tsallis entropy, we obtain an equation of the state known as stellar polytrope. Considering the self-gravitating stellar system confined within a perfectly reflecting wall, its thermodynamical instability caused by a negative specific heat is discussed. And a role of the extremum as a quasi-equilibrium is shown from results of N-body simulations.

**Key words:** non-extensive entropy, self-gravitating system, gravothermal instability, negative specific heat, stellar polytrope

**PACS:** 98.10.+z, 05.70.Ln, 05.20.-y

### 1 Introduction

In any subject of astrophysics and cosmology, many-body gravitating systems play an essential role. We know that globular clusters and elliptical galaxies, which are recognized as self-gravitating stellar systems, are their typical examples [1,2,3,4]. Several beautiful works on thermodynamics of self-gravitating systems [5,6] have shown their peculiar features such as a negative specific heat and an absence of global entropy maximum, which is referred to as the gravothermal catastrophe (for general introduction on this subject, see [7]). Furthermore the long-range nature of the gravitational interaction often tempts us to discuss a relationship between non-extensive thermodynamics and the self-gravitating systems.

Recently, a new framework of thermodynamics based on Tsallis' non-extensive entropy has been proposed [8]. And its application has been extensively discussed to deal with a variety of interesting problems to which the standard Boltzmann-Gibbs statistical mechanics could not be applied [9,10]. Among these subjects for the Tsallis' framework of thermodynamics, the self-gravitating stellar system seems to be the most interesting one (e.g., [11,12,13]). Here some progresses in the application to the stellar system [14,15,16,17] will be reviewed. Although its dynamics is complicated in general, if we impose spherical symmetry to the system, its treatment is considerably simplified due to well-known  $1=r^2$  behavior of the gravitational force. Furthermore the spherical system still keeps its remarkable nature of the negative specific heat [6]. Thus the self-gravitating stellar system seems to be a desirable testing ground for Tsallis' non-extensive thermodynamics.

---

Correspondence to: M. Sakagami (e-mail: sakagam@phys.h.kyoto-u.ac.jp) A. Taruya (e-mail: atanuya@utap.phys.s.u-tokyo.ac.jp)

This paper is organized as follows. In section 2, we briefly review typical nature of the self-gravitating systems. Especially, a standard treatment for the gravothermal catastrophe based on the Boltzmann-Gibbs entropy is explained. Then its extension to the Tsallis entropy is discussed in section 3. The properties of states of the stellar system which extremize Tsallis entropy are clarified. In section 4, an interesting role of the above states as quasi-equilibrium is discussed from results of numerical simulation. Finally, section 5 is devoted to conclusion and discussion.

## 2 Some basic properties of the self-gravitating systems

In order to get intuitive comprehension for evolution of the many-body self-gravitating systems, let us consider a very simple situation: a circular motion of a particle of a mass  $m$  and a velocity  $v$  at a radius  $r$  in a spherical mass distribution with a constant density  $\rho_0$ .

$$m \frac{v^2}{r} = \frac{G m M(r)}{r^2}; \quad M(r) = \frac{4}{3} \pi r^3 \rho_0 \quad (2.1)$$

where  $G$  is the gravitational constant and  $M(r)$  is a mass contained within a sphere of a radius  $r$ . By means of an orbital period  $T$ , we define the dynamical time of the system (e.g. p.57 of ref.[1]) as

$$t_{\text{dyn}} = \frac{T}{4} = \frac{r}{\sqrt{\frac{3}{16 G \rho_0}}}; \quad (2.2)$$

which is recognized as a characteristic time scale of more general self-gravitating systems with mean density  $\rho_0$ . A distribution of the self-gravitating system evolves with the time scale (2.2) so that it is called the dynamical time. As explained in the appendix, the many-body self-gravitating system has another time scale, i.e. the relaxation time [18] (see also chapter 4 of ref. [1]),

$$t_{\text{rel}} = \frac{0.1 N}{\ln N} t_{\text{dyn}} \quad (2.3)$$

where  $N$  is a number of particles in the system. This time scale represents the relaxation processes due to scattering by gravitational interaction between each pair of particles.

In a usual system, we believe that a distribution of particles approaches the so-called thermal equilibrium state within the relaxation time (2.3). However, this is not necessarily the case for the self-gravitating systems, since it has a peculiar nature of a negative specific heat, which is explained through the following discussion. For the circular orbit obeying (2.1), the virial theorem is easily derived as

$$2K + U = 0; \quad (2.4)$$

where  $K = m v^2/2$  is the kinetic and  $U = -G m M(r)/r$  the potential energies, respectively. In general self-gravitating many-body systems which consists of  $N$  particles, the virial relation same as (2.4) holds between a long time averaged values of the total kinetic and the total potential energy (e.g. see chapter 8.1 of ref.[1]). Thus the total energy  $E$  can be expressed as

$$E = K + U = -K: \quad (2.5)$$

If we introduce a temperature to characterize the total kinetic energy as  $K = 3N kT/2$  where  $k$  is the Boltzmann constant, then the equation (2.5) tells us that the specific heat of self-gravitating systems is negative,

$$C = \frac{dE}{dT} = -\frac{3N k}{2} < 0; \quad (2.6)$$

which suggests the existence of the thermodynamical instability proceeding with the relaxation time scale (2.3).

For a precise discussion of the thermodynamical properties of the self-gravitating systems, Antonov [5] and Lynden-Bell and Wood [6] considered a system confined within a spherical adiabatic wall of a radius  $r_e$ . This means that the  $N$  particles in this system interact via Newton gravity and bounce elastically from the wall. In order to investigate equilibrium states of the system, the Boltzmann-Gibbs entropy of the system

$$S_{BG} = \frac{1}{Z} \ln \int d^6 p \, f^N \ln f^N; \quad (2.7)$$

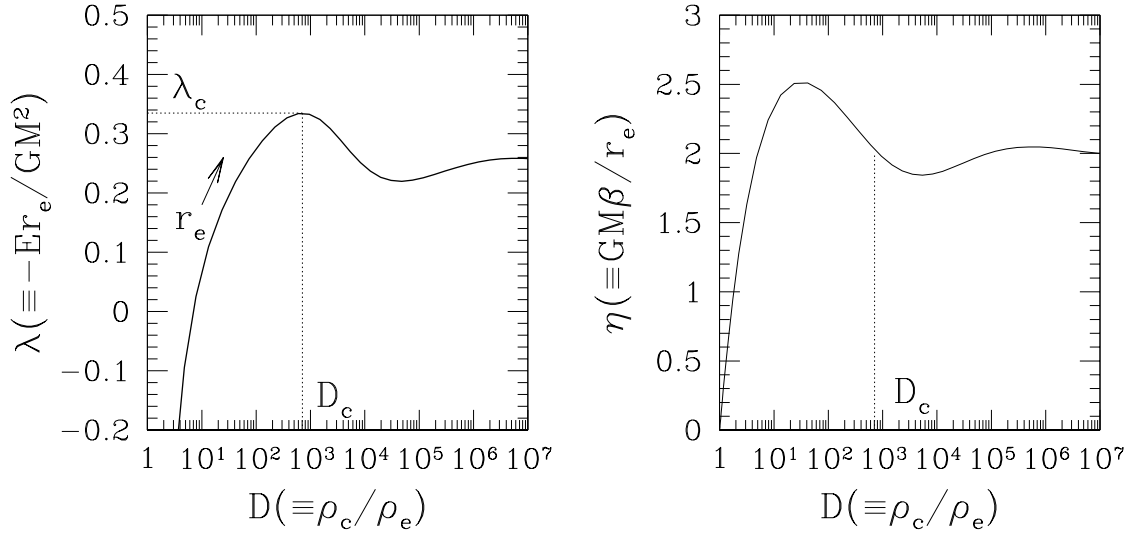


Fig. 2.1. Energy-radius-density contrast (left) and radius-temperature-density contrast (right) relationships for the isothermal stellar system.

is introduced, where  $f(x; v)$  is the distribution function in phase-space. Here the phase space measure is defined as

$$d^6 \frac{d^3x d^3v}{h^3}; \quad h^3 = (l_0 v_0)^3 \quad (2.8)$$

where  $h^3$  denotes the phase space element with unit length  $l_0$  and unit velocity  $v_0$ . Hereafter we set the Boltzmann constant to be unity, i.e.  $k = 1$ . Under a condition that the total mass  $M$  and the energy  $E$  of the system are kept constant, we maximize the entropy  $S_{BG}$ ,

$$S_{BG} \quad M \quad E = 0 \quad (2.9)$$

where and are Lagrange multipliers. Through this procedure, an equation of state of the system turns to be isothermal [6],

$$\begin{aligned} p(x) &= \frac{1}{3} v^2 f \frac{d^3v}{h^3} = \frac{f(x)}{Z}; \\ f(x) &= \frac{d^3v}{h^3} \end{aligned} \quad (2.10)$$

where  $p$  and are pressure and density, respectively. In ordinary systems, their thermal equilibrium states are homogeneous, i.e. having a uniform density. However this is not the case for the self-gravitating systems. For spherical systems we are discussing here, the amplitude of the density and the pressure should increases as decreasing the radius  $r$  in order to support the system against its self-gravity. It is shown that a series of equilibrium states is well parameterized by a value of the density contrast  $D = \rho_c/\rho_e$ , where  $\rho_c$  is a central density and  $\rho_e = (r_e)$  means the density at the wall. In the next section, we will present the procedures of the calculation for the equilibrium state in more general situation. In fig. 2.1 (left), we plot the dimensionless quantity  $\lambda = -r_e E/GM^2$  as a function of the density contrast  $D$ . Since the solid curve in this figure represents states which extremize the entropy, we note that no equilibrium state is attained, when the radius of the wall  $r_e$  is larger than the critical radius

$$r_c = 0.335 \frac{GM^2}{(E)}; \quad (2.11)$$

which corresponds to the state with the critical density contrast  $D_c = 709$ . Furthermore it can be shown that, along the curve  $(D)$  derived from the condition  $S_{BG} = 0$ , all states with  $D > D_c$  are unstable from the turning point analysis for a linear series of equilibria [6, 19, 20, 21]. Also, the explicit

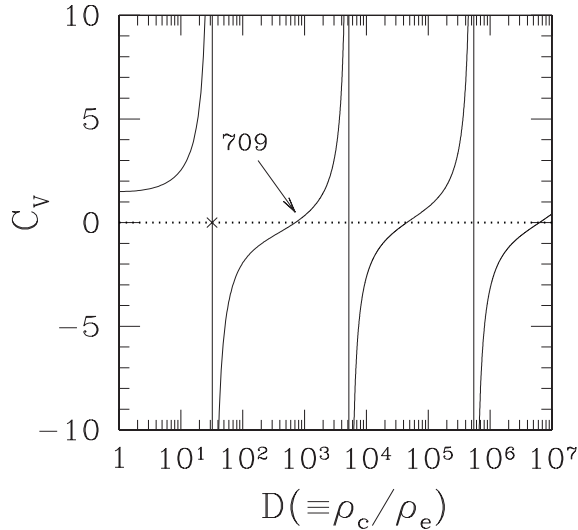


Fig. 2.2. Specific heat as a function of the density contrast  $D = \rho_c / \rho_e$  for the isotropic stellar system.

evaluation of the eigenmodes for the second variation of the entropy  $S_{BG}^2$  leads to the same results [7,19]. We call these phenomena, i.e. the absence of the thermal equilibrium in self-gravitating systems when  $r > r_c$  and/or  $D > D_c$ , the gravothermal catastrophe.

Heuristically, this instability is explained by the presence of negative specific heat as follows. In a fully relaxed gravitating system with sufficiently larger radius, negative specific heat arises at the inner part of the system and we have  $C_V, \text{inner} < 0$ , while the specific heat at the outer part remains positive,  $C_V, \text{outer} > 0$ , since one can safely neglect the effect of self-gravity. In this situation, if a tiny heat flow is momentarily supplied from inner to outer part, both the inner and the outer parts get hotter after the readjustment of the system. Now imagine the case,  $C_V, \text{outer} > |C_V, \text{inner}|$ . The outer part has so much thermal inertia that it cannot heat up as fast as the inner part, and thereby the temperature difference between inner and outer parts increases. As a consequence, the heat flow never stops, leading to a catastrophe temperature growth.

The Fig. 2.1 (right) plots the dimensionless inverse temperature  $GM = r_e$  with respect to the density contrast. Then we can evaluate the specific heat at constant volume,

$$C_V = \frac{dE}{dT} \Big|_{r_e} = M^2 \frac{dE}{dD} \Big|_{r_e} = M^2 \frac{\frac{d}{dD} \Big|_{r_e}}{\frac{d}{dD} \Big|_{r_e}} : \quad (2.12)$$

as shown in the Fig. 2.2.

In contrast to the naive discussion for (2.6) based on the virial theorem, the actual specific heat (2.12) changes its sign many times. We observe that the self-gravitating system confined by wall of smaller radius has a positive specific heat. The reason is as follows. It can be shown that the virial theorem for the system surrounded by a boundary leads not to (2.4) but to

$$2K + U = 3P_e V; \quad (2.13)$$

where  $P_e$  is the pressure at the wall and  $V$  the volume of the system (e.g., see eq.(29) of the paper [14]). For the case of a smaller radius, the surface energy dominates the gravitational energy of the bulk so that the system behaves as a normal one, i.e.  $C_V > 0$ . As the radius  $r_e$  increases, the gravitational energy becomes significant. Eventually the specific heat changes its sign,  $C_V < 0$ , when the value of the density contrast becomes  $D = 32.2$ , which corresponds to a peak of  $(D)$  curve (the left of Fig. 2.1).

At the onset of the gravothermal catastrophe,  $D_c = 709$ , the specific heat vanishes, and  $C_V > 0$  in the unstable segment of  $(D)$  curve,  $D > 709$ . This fact implicitly indicates a role of the negative specific heat to the existence of thermodynamical instability in the self-gravitating system. Following

the previous heuristic argument, above the critical point  $D > D_c = 709$ , the specific heat of the total system becomes positive,  $C_V = C_{V,inner} + C_{V,outer} > 0$ , equivalently

$$C_{V,outer} > C_{V,inner} > 0; \quad (2.14)$$

which means the outer normal part of the system has much heat capacity so that it cannot catch up with the temperature increase of the inner part.

So far, we have discussed some interesting features of the self-gravitating systems. Among these properties, peculiarity of the system arising from the negative specific heat has been studied in terms of the Boltzmann-Gibbs entropy (2.7). In the next section, this sort of the analysis will be extended to that based on the non-additive entropy, i.e. Tsallis entropy. However, before closing this section, we briefly summarize succeeding investigation on the gravothermal catastrophe.

In this paper we adopt the thermodynamical approach in terms of the entropy and/or the free energy in order to investigate instabilities of the self-gravitating systems. Although this method has an advantage of its simplicity, we cannot deal with the dynamical aspect of the instability appearing in the relaxation time scale (2.3). Typically, each particle (star) in self-gravitating system has a long mean free path comparing to its system size. In other words, during its travel across the system, the particle motion is driven by the gravitational potential of the whole system and the particle experiences quite few number of 2-body encounters so that the relaxation time  $t_{rel}$  (2.3) is much longer than the dynamical one  $t_{dyn}$  (2.2). This means that we cannot rely on the usual notion of the local equilibrium, which is realized in the cases with a short mean free path. Thus, the Fokker-Planck equation (e.g. see chapter 8.3 of ref.[1]), which can be derived from the expansion of a collision integral in the Boltzmann equation with respect to the momentum transfer due to the 2-body collision, is the useful approach to study the long-term evolution of the self-gravitating system. By means of the linearized Fokker-Planck equation, eigenvalues and eigenfunctions which describe the time evolution of the perturbation around the thermal equilibrium have been obtained [22].

On the other hand, the gas model where a star (particle) in the self-gravitating many-body system is replaced with a gas particle is an alternative approach. Although the gas model loses some typical nature of the self-gravitating many-body system, we note that it still shows the interesting aspects of the gravothermal catastrophe. In this model, the local relaxation time is shorter than the dynamical time scale. Thus, we can introduce usual notions of the local equilibrium and the local temperature, which make our analysis much easier than the stellar system. The local specific heat is evaluated to show that the condition (2.14) characterizes the onset of the gravothermal catastrophe [23]. And the time evolution of the linear perturbation around the equilibrium gas with heat transfer is investigated to show that the proposed mechanism for the instability based on the negative specific heat actually works in the self-gravitating gaseous systems [24].

### 3 Analysis of gravothermal catastrophe based on Tsallis' generalized entropy

#### 3.1 Tsallis entropy and stellar polytrope

Here we shall discuss a generalization of the analysis in previous section based on the Boltzmann-Gibbs entropy (2.7) to the case of Tsallis entropy. Its details are shown in the literatures [4, 15, 16]. Regarding the function  $f(x; v)$  as a one-particle distribution, the energy and the mass are respectively expressed as follows:

$$E = K + U = \frac{1}{2} v^2 + \frac{1}{2} \langle x \rangle f(x; v) d^6; \quad (3.1)$$

$$M = f(x; v) d^6; \quad (3.2)$$

where the quantity  $\langle x \rangle$  is the gravitational potential given by

$$\langle x \rangle = G \frac{\int_{\mathbb{R}^3} f(x^0; v^0) d^6 v^0}{\int_{\mathbb{R}^3} d^6 v^0}; \quad (3.3)$$

As for generalization, the most crucial problem is the choice of the statistical average in non-extensive thermodynamics. Following a seminal paper by [11], the analyses in a couple of our paper [14, 15] have been done utilizing the old Tsalis formalism with the standard linear mean values (see also [25, 26] for comparative works). On the other hand, a more sophisticated framework by means of the normalized  $q$ -expectation values has been recently presented [27, 28]. As several authors advocated, the analysis using normalized  $q$ -expectation values is thought to be essential, since the undesirable divergences in some physical systems can be eliminated safely when introducing the normalized  $q$ -expectation values. Further, non-uniqueness of the Boltzmann-Gibbs theory has been shown using the normalized  $q$ -expectation values [29]. In this paper, we mainly report our investigation [16] based on the normalized  $q$ -expectation values. However, this does not imply that all the analyses with standard linear means or un-normalized  $q$ -expectation values lose the physical significance. Actually we could observe some differences between results based on both frameworks, which will be mentioned at the end of this section.

In the new framework of Tsalis' non-extensive thermodynamics, all the macroscopic observables of the quasi-equilibrium system can be characterized by the escort distribution, but the escort distribution itself is not thought to be fundamental. Rather, there exists a more fundamental probability function  $p(x;v)$  that quantifies the phase-space structure. With a help of this function, the escort distribution is defined and the macroscopic observables are expressed as the normalized  $q$ -expectation value as follows (e.g., refs. [27, 28]):

$$\text{escort distribution} : P_q(x;v) = \frac{Z}{d^6} \frac{fp(x;v)g^q}{\int fp(x;v)g^q} ; \quad (3.4)$$

$$\text{normalized } q\text{-value} : H_{\text{q}} = \frac{Z}{d^6} \int P_q(x;v) : \quad (3.5)$$

And based on the fundamental probability  $p(x;v)$ , the Tsalis entropy is given by

$$S_q = \frac{1}{q-1} \int d^6 \left[ fp(x;v)g^q - p(x;v) \right] : \quad (3.6)$$

Note that the probability  $p(x;v)$  satisfies the normalization condition:

$$\int d^6 p(x;v) = 1 : \quad (3.7)$$

To apply the above Tsalis formalism to the present problem without changing the definition of energy and mass (3.1) and (3.2), we identify the one-particle distribution with the escort distribution  $P_q$ , not the probability function  $p(x;v)$ :

$$f(x;v) = M \frac{fp(x;v)g^q}{N_q} ; \quad N_q = \int d^6 fp(x;v)g^q : \quad (3.8)$$

so as to satisfy the mass conservation (3.2). The definitions of the Tsalis entropy (3.6) and the escort distribution (3.8) clearly show that the Boltzmann-Gibbs entropy (2.7) is recovered in the limit  $q \rightarrow 1$ . Now, adopting the relation (3.8), let us seek the extremum-entropy state under the constraints (3.1) and (3.7). The variational problem is given by the following equation:

$$S_q = \int d^6 p \left[ 1 - \int d^6 \left( \frac{1}{2} v^2 + \frac{1}{2} f \right) E \right] = 0 ; \quad (3.9)$$

where the variables  $\lambda$  and  $\mu$  denote the Lagrange multipliers. The variation with respect to the probability  $p(x;v)$  gives the extremum-entropy state so-called stellar polytrope [16] (see also p.223 of ref. [1])

$$f(x;v) = M \frac{fp(x;v)g^q}{N_q} = A \lambda_0 \left( \frac{1}{2} v^2 + \frac{1}{2} f \right)^{q/(1-q)} ; \quad (3.10)$$

where we define the constants  $A$  and  $\lambda_0$  as follows:

$$A = \frac{M}{N_q} = \frac{q(1-q)}{(1-q)+1} \frac{M}{N_q} ; \quad \lambda_0 = \frac{N_q}{M(1-q)} + < " > ; \quad (3.11)$$

with the quantity  $\langle \cdot \rangle$  being

$$\langle \cdot \rangle = \frac{1}{M} \int_0^Z d^6x \cdot \frac{1}{2} v^2 + f: \quad (3.12)$$

By means of the distribution function (3.10), we evaluate the density  $\rho(r)$  and the isotropic pressure  $P(r)$  at the radius  $r = \sqrt{x}$  as

$$\begin{aligned} \rho(r) &= \frac{Z}{h^3} \int d^3v f(x; v); \\ &= \frac{p}{4} \frac{1}{2} B\left(\frac{3}{2}; \frac{1}{1-q}\right) \frac{A}{h^3} [0 \quad \langle r \rangle]^{1-(1-q)+1=2} \end{aligned} \quad (3.13)$$

and

$$\begin{aligned} P(r) &= \frac{Z}{h^3} \frac{1}{3} v^2 f(x; v); \\ &= \frac{p}{3} \frac{1}{2} B\left(\frac{5}{2}; \frac{1}{1-q}\right) \frac{A}{h^3} [0 \quad \langle r \rangle]^{1-(1-q)+3=2}; \end{aligned} \quad (3.14)$$

Here, the function  $B(a; b)$  denotes the beta function. These two equations lead to the following polytropic relation:

$$P(r) = K_n^{1+1/n} \rho(r); \quad (3.15)$$

with the polytrope index  $n$  related to the parameter  $q$

$$n = \frac{1}{1-q} + \frac{1}{2}; \quad (3.16)$$

And the explicit form of the dimensional constant  $K_n$  is given in [16]. We note that the isothermal equation of the state (2.10) discussed in the previous section arises in the limit  $n \rightarrow 1$  ( $q \rightarrow 1$ ) as expected.

In terms of  $K_n$  and  $\rho$ , the one-particle distribution can be rewritten as follows:

$$f(x; v) = \frac{1}{4} \frac{p}{2} B(3=2; n=1=2) \frac{h^3}{f(n+1) K_n^{1=n} g^{3=2}} \frac{1}{1 - \frac{v^2=2}{(n+1) K_n^{1=n}}}; \quad (3.17)$$

which agrees with the result based on old T salis formalism. That is to say, the equilibrium distribution (3.17) turns out to be invariant irrespective of the choice of the statistical averages.

We note that the equilibrium distribution (3.10) with (3.11) contains the new quantities  $N_q$  and  $\langle \cdot \rangle$ , which implicitly depend on the distribution function itself. In marked contrast to the result in old T salis formalism, this fact gives rise to the non-trivial thermodynamic relations as follows. Using the definitions of density and pressure (3.13) and (3.14), the quantity  $\langle \cdot \rangle$  becomes

$$\begin{aligned} \langle \cdot \rangle &= \frac{1}{M} \int_0^Z d^3x P(x) + \int_0^Z d^3x \langle x \rangle (x) \\ &= \frac{1}{M} \int_0^Z d^3x P(x) \int_0^Z d^3x \langle x \rangle (x) + \langle x \rangle_0; \end{aligned}$$

Further using the relation  $\langle x \rangle_0 = (n+1) \langle P \rangle_0$  from (3.13) and (3.14) and substituting the equation (3.11) into the above expression, the quantity  $\langle \cdot \rangle$  is canceled and the equation reduces to

$$\frac{N_q}{Z} = \int_0^Z d^3x P(x); \quad (3.18)$$

As for  $N_q$ , the normalization condition (3.7) gives us its actual expression [16].

### 3.2 Gravothermal catastrophe in stellar polytropic system

We will specifically focus on the spherically symmetric case with the polytrope index  $n > 3=2$  ( $q > 0$ ), in which the equilibrium distribution is at least dynamically stable (see chapter 5 of ref.[1]). In this case, the stellar equilibrium distribution can be characterized by the so-called Emden solutions (e.g., [30,31]) and all the physical quantities are expressed in terms of the homology invariant variables  $(u; v)$ , which are subsequently used in later analysis.

We note that the one-particle distribution function (3.10) does not yet completely specify the equilibrium configuration, due to the presence of gravitational potential which implicitly depends on the distribution function itself. Hence, we need to specify the gravitational potential or density profile. From the gravitational potential (3.3), we obtain the Poisson equation

$$\frac{1}{r^2} \frac{d}{dr} r^2 \frac{d \phi(r)}{dr} = 4 \pi G \rho(r); \quad (3.19)$$

Combining the above equation with (3.13), we obtain the ordinary differential equation for  $\rho$ . Alternatively, a set of equations which represent the hydrostatic equilibrium are derived using (3.19), (3.13) and (3.14):

$$\frac{dP(r)}{dr} = -\frac{Gm(r)}{r^2} \rho(r); \quad (3.20)$$

$$\frac{dm(r)}{dr} = 4\pi(r) r^2 \rho(r); \quad (3.21)$$

The quantity  $m(r)$  denotes the mass evaluated at the radius  $r$  inside the wall. Denoting the central density and pressure by  $\rho_c$  and  $P_c$ , we then introduce the dimensionless quantities:

$$= \rho_c [(\rho)]^{\frac{1}{n+1}}; \quad r = \frac{(n+1)P_c}{4\pi G \rho_c^{\frac{2}{n+1}}} r^{\frac{1}{n+1}}; \quad (3.22)$$

which yields the following ordinary differential equation:

$$\omega + \frac{2}{n+1} \rho' + \rho^{\frac{n}{n+1}} = 0; \quad (3.23)$$

where prime denotes the derivative with respect to  $r$ . The quantities  $\rho_c$  and  $P_c$  in (3.22) are the density and the pressure at  $r = 0$ , respectively. To obtain the physically relevant solution of (3.23), we put the following boundary condition:

$$\rho(0) = 1; \quad \rho'(0) = 0; \quad (3.24)$$

A family of solutions satisfying (3.24) is referred to as the Emden solution, which is well-known in the subject of stellar structure (e.g., see chapter IV of ref.[30]). To characterize the equilibrium properties of Emden solutions, it is convenient to introduce the following set of variables, referred to as homology invariants [30,31]:

$$u = \frac{d \ln m(r)}{d \ln r} = \frac{4 \pi r^3 \rho(r)}{m(r)} = -\frac{n}{\rho}; \quad (3.25)$$

$$v = \frac{d \ln P(r)}{d \ln r} = \frac{\rho(r)}{P(r)} \frac{Gm(r)}{r} = -(n+1) \frac{\rho}{\rho}; \quad (3.26)$$

which reduce the degree of equation (3.23) from two to one. And remember that we investigate the thermodynamical properties of the self-gravitating system within the wall of the radius  $r_e$ . We can evaluate the total energy of the confined stellar system in terms of the pressure  $P_e$ , the density  $\rho_e$  at the boundary  $r_e$  and the total mass  $M$

$$\begin{aligned} E = K + U &= \frac{3}{2} \int_0^{r_e} dr 4 \pi r^2 P(r) + \int_0^{r_e} dt \frac{Gm(r)}{r} \frac{dm}{dr} \\ &= \frac{1}{n-5} \frac{3}{2} \frac{GM^2}{r_e} + (n+1) \frac{M P_e}{r_e} + (n-2) 4 \pi r_e^3 P_e; \end{aligned}$$

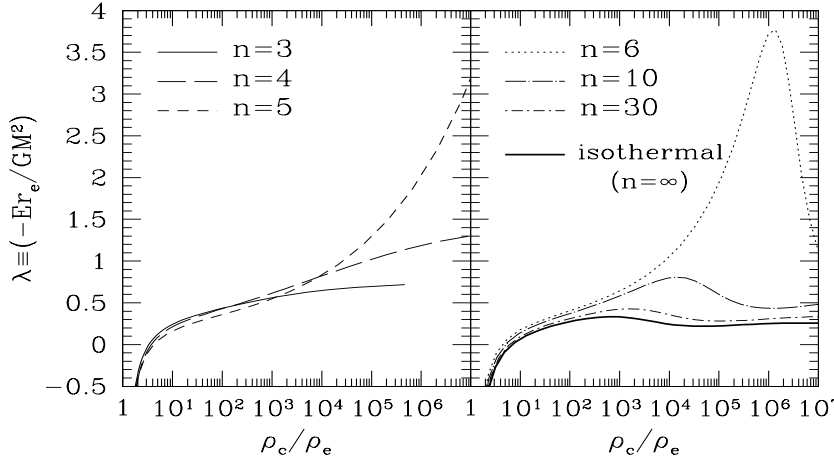


Fig. 3.1. Energy-radius-density contrast relationship for the stellar polytropes with various indices.

by which the dimensionless quantity can be expressed as a function of the homology invariants at the wall [14,15,16] :

$$\frac{E r_e}{G M^2} = \frac{1}{n-5} \left( \frac{3}{2} \right)^{\frac{1}{n-1}} \left( \frac{n+1}{v_e} \right)^{\frac{n+1}{n-1}} + (n-2) \frac{u_e}{v_e} : \quad (3.27)$$

As was already shown in the section 2 for the isothermal case, the above dimensionless quantity has an important role for the analysis of the gravothermal catastrophe. Figure 3.1 shows as a function of the ratio of the central density to that at the boundary,  $\rho_c / \rho_e$ . We notice that  $\lambda$ -curves are bounded from above and have peaks in the case of  $n > 5$  (right panel). On the other hand, curves for  $n \leq 5$  monotonically increase (left panel). It follows that the stellar polytrope within an adiabatic wall exhibits the gravothermal instability in the case of the polytropic index  $n > 5$ . Similarly to the isothermal case, the evaluation of eigenvalues for the second variation of the Tsallis entropy  $^2S_q$  derives same results as the above turning point analysis in terms of the  $\lambda$ -curve [14,15,16].

### 3.3 Thermodynamic instability arising from the negative specific heat

As discussed in the isothermal case in the previous section, the thermodynamic instability in stellar system is intimately related to the presence of negative specific heat [32]. The evaluation of specific heat is thus necessary for clarifying the thermodynamic property. In this regard, the identification of temperature in stellar system in the polytropic case is the most essential task.

In the new framework of Tsallis' non-extensive thermodynamics, the physically plausible thermodynamic temperature,  $T_{\text{phys}}$ , can be defined from the zero-th law of thermodynamics [3,34,35]. Then, the thermodynamic temperature in non-extensive system differs from the usual one, i.e., the inverse of the Lagrange multiplier,  $\beta$ . The pseudo-additivity of the Tsallis entropy and the transitivity of thermal equilibrium suggests

$$T_{\text{phys}} = [1 + (1-q) S_q]^{-1} : \quad (3.28)$$

Here, the relation (3.28) should be carefully applied to the present case, since the verification of thermodynamic zero-th law is very difficult in stellar equilibrium system with long-range interaction. Furthermore, even using the new formalism, the energy  $E$  still keeps non-extensive due to the self-referential form of the potential energy (see Eqs.(3.1)-(3.3)). However the consistency of the physical temperature given by (3.28) can be shown by the alternative argument [15,16] in the self-gravitating stellar system, where the modified Clausius relation [3,34,35]

$$dS_q = \frac{1}{T_{\text{phys}}} f_1 + (1-q) S_q g d^0 Q :$$

play a significant role.

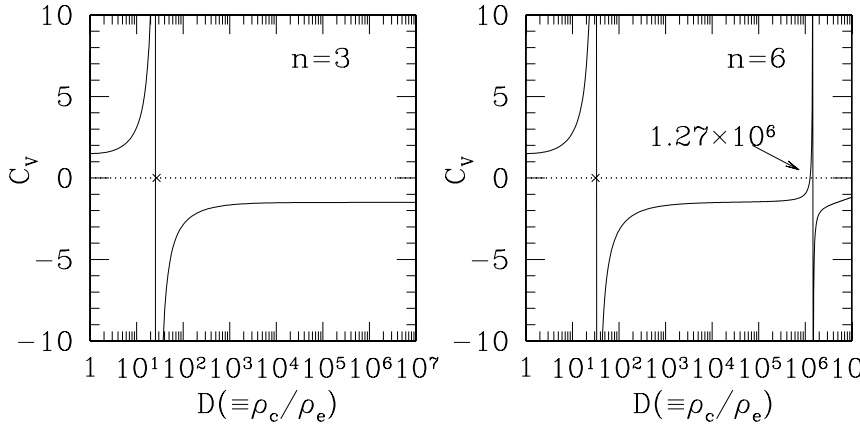


Fig. 3.2. Specific heat as a function of the density contrast for the stellar polytropes with  $n = 3$  (left) and  $n = 6$  (right).

From the expression of the normalization factor  $N_q$  of the escort distribution (3.8), the  $T_{\text{Sallis}}$  entropy (3.6) of extremum state is given by

$$S_q = \frac{1}{1-q} (N_q - 1):$$

Let us substitute this expression into (3.28). Then the relation (3.18) for  $N_q = 1$  gives us the expression of the thermodynamical temperature  $T_{\text{phys}}$  as an integral of the physical quantity, i.e. the pressure distribution:

$$T_{\text{phys}} = \frac{N_q}{Z} = \int d^3x P(x): \quad (3.29)$$

We can evaluate the above integral to represent the thermodynamical temperature in terms of the pressure  $P_e$ , the density  $\rho_e$  at the boundary and the total mass  $M$  as

$$T_{\text{phys}} = \frac{1}{n-5} 8 \pi r_e^3 P_e (n+1) \frac{M P_e}{r_e} + \frac{G M^2}{r_e} \quad (3.30)$$

by which the dimensionless inverse temperature is denoted in a form

$$\frac{G M^2}{r_e T_{\text{phys}}} = \frac{(n-5) v_e}{n+1 - 2u_e - v_e} \quad (3.31)$$

as a function of the homology invariant at the boundary [16]. From (3.27) and (3.31), the specific heat at the constant volume  $C_v$  is given by

$$C_v = \frac{dE}{dT_{\text{phys}}} \Big|_e = \frac{d}{d \frac{1}{r_e}} \Big|_e: \quad (3.32)$$

In order to compare with the behavior of the specific heat in the isothermal case of Fig. 2.2, we plot  $C_v$  with respect to the density contrast for several values of the polytropic index in Fig. 3.2.

As already denoted in the end of subsection 3.2, the stellar polytropic system exhibits the gravothermal catastrophe, when the polytropic index  $n$  is larger than the critical value, i.e.  $n > 5$ . In the isothermal case, the onset of the thermodynamical instability is characterized by the condition (2.14). Figure 3.3 shows that the thermodynamical argument based on the negative specific heat for the gravothermal catastrophe can extend to the cases of the stellar polytrope, i.e. the equilibrium of the self-gravitating system described by the extremum of the  $T_{\text{Sallis}}$  entropy.

In Fig. 3.3, we depict the density profiles with respect to the dimensionless radius (3.22). Clearly, profiles with index  $n < 5$  rapidly fall off and they abruptly terminate at finite radius (left-panel), while the  $n = 5$  cases nicely continue to extend over the outer radius (right-panel). It follows that the stellar polytropic system with index  $n = 5$  are able to possess sufficient amount of outer norm apart to realize the gravothermal catastrophe.

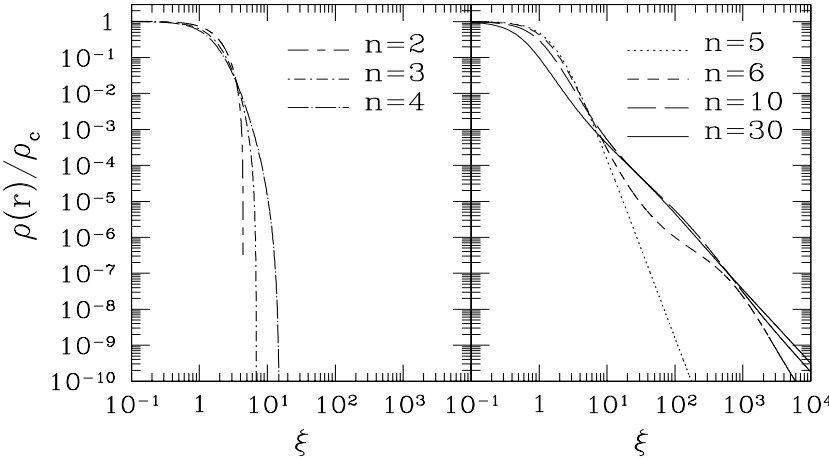


Fig. 3.3. Density profiles of the stellar polytropes for  $n < 5$  (left) and  $n = 5$  (right).

Before closing this section, we mention differences between the old and new Tsalis formalisms. First, the relation between the polytrope index  $n$  and Tsalis parameter  $q$  in the polytropic relation (3.16) differs from the one obtained previously, but is related to it through the duality transformation,  $q \neq 1 = q$  (see Eq.(14) in ref.[14] or Eq.(12) in ref.[15]). This property has been first addressed in Ref.[7] in more general context, together with the changes in Lagrangian multiplier. The duality relation implies that all of the thermodynamical properties in the new formalism can also be translated into those obtained in the old formalism. Second, in previous studies [15] based on the standard linear means, the radius-mass-temperature relation and the specific heat seriously depend on the dimensional parameter for the phase element  $h$  (2.8). By contrast, in present case [16], the radius-mass-temperature relation was derived from the non-trivial relation (3.18), in which no such  $h$ -dependence appears. The resultant specific heat is also free from this dependence, which is a natural outcome of the new framework using the normalized  $q$ -expectation values. Therefore, it seems likely that the new formalism provides a better characterization for non-extensive quasi-equilibrium systems.

#### 4 Reality of stellar polytrope as a quasi-equilibrium state

So far we have discussed the extension of thermodynamical analysis to the stellar polytrope which is obtained by applying the variational procedure to the Tsalis entropy for the stellar self-gravitating system. It has been shown that the thermodynamical quantities such as the specific heat are useful to study the emergence of the gravothermal catastrophe in the stellar polytrope. In Fig. 4.1 we summarize our results. The stellar polytrope confined in an adiabatic wall is shown to be thermodynamically stable when the polytrope index  $n < 5$ . In other words, if  $n > 5$ , a stable equilibrium state ceases to exist for a sufficiently large density contrast  $D > D_{\text{crit}}$ , where the critical value  $D_{\text{crit}}$  given by a function of  $n$  is determined from the second variation of entropy around the extremum state of Tsalis entropy,  ${}^2S_q = 0$  [14,16]. The dotted line in Fig. 4.1 represents the critical value  $D_{\text{crit}}$  for each polytrope index, which indicates that the stellar polytrope at low density contrast  $D < D_{\text{crit}}$  is expected to remain stable.

The above arguments indicate that, similar to the isothermal state, the stellar polytropic distribution can be also regarded as an equilibrium state, since it is described by the extremal state of the Tsalis entropy. However, the one-particle distribution function of the stellar polytrope (3.17) clearly shows that the velocity dispersion

$$\langle v^2 \rangle = \frac{1}{\langle r \rangle} \int_0^{\infty} \frac{d^3v}{h^3} v^2 f(x; v); \quad (4.1)$$

depends on the radius  $r$ . Only in the isothermal case  $n = 1$ , it is kept spatially constant. Thus it is expected that a gradient of the velocity dispersion is relaxed within the time scale due to 2-body collisions (2.3). This means that the stellar polytrope is no longer the equilibrium but quasi-equilibrium

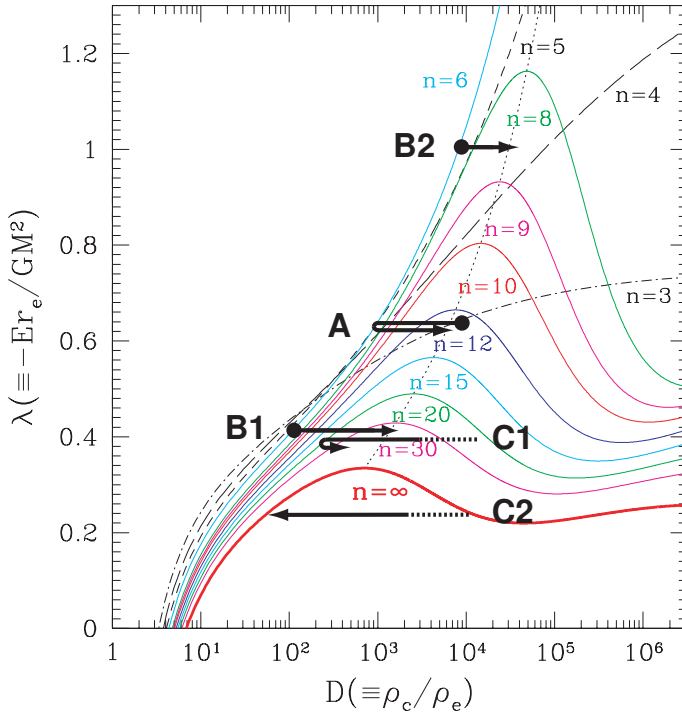


Fig. 4.1. Equilibrium sequences of stellar polytrope and isothermal distribution ( $n = 1$ ) in  $r_e E = (GM^2)$  vs  $D = \rho_c/\rho_e$  plane. The thick arrows denote the evolutionary tracks in each simulation run (see Sec.4).

state. In this section, we report the results of the  $N$ -body simulations [17] which are carried out to investigate how the stellar polytrope actually evolves.

The  $N$ -body experiment considered here is in the same situation as investigated in classic papers ([5,6], see also Ref. [36]). That is, we confine the  $N$  particles interacting via Newton gravity in a spherical adiabatic wall, which reverses the radial components of the velocity if the particles reach the wall. Without loss of generality, we set the units as  $G = M = r_e = 1$ . Note that the typical timescales appearing in this system are the dynamical time,  $t_{\text{dyn}}$  (2.2), and the global relaxation time driven by the two-body encounter,  $t_{\text{rel}}$  (2.3), which are basically scaled as  $t_{\text{dyn}} \sim 1$  and  $t_{\text{rel}} \sim 0.1N = \ln N$  in our units. Table 4.1 summarizes the list of the five simulation runs. Here, in addition to the stellar polytropic initial state, we also consider the non-stellar polytropic state of the Hernquist model [37], which was originally introduced to account for the empirical law of observed elliptical galaxies [1].

As was expected, the numerical simulations reveal that the stellar polytropic distribution gradually changes with time, on the timescale of two-body relaxation (2.3). Furthermore, focusing on the evolutionary sequence, we found that the transient state starting from the initial stellar polytrope can be remarkably characterized by a sequence of stellar polytropes (run A, B1 and B2). This is even true in the case starting from the Hernquist model (run C1).

Let us show the representative results taken from run A (Fig. 4.2). Fig. 4.2(a) plots the snapshots of the density profile ( $r$ ), while Fig. 4.2(b) represents the distribution function  $f(\mathbf{v})$  as a function of the specific energy  $\mathbf{v}^2/2 + \phi(\mathbf{x})$ . Note that just for illustrative purpose, each output result is artificially shifted to the two-digits below. Only the final output with  $T = 400$  represents the correct scales. In each figure, solid lines mean the initial stellar polytrope with  $n = 3$  and the other lines

Table 4.1. Initial distributions and their evolutionary states

run no.	initial distribution	parameters	no. of particles	transient state	final state
A	stellar polytrope ( $n = 3$ )	$D = 10,000$	2,048	stellar polytrope	collapse
B1	stellar polytrope ( $n = 6$ )	$D = 110$	2,048	stellar polytrope	collapse
B2	stellar polytrope ( $n = 6$ )	$D = 10,000$	2,048	stellar polytrope	collapse
C1	Hernquist model	$a = r_e = 0.5$	8,192	stellar polytrope	collapse
C2	Hernquist model	$a = r_e = 1.0$	8,192	none	isothermal

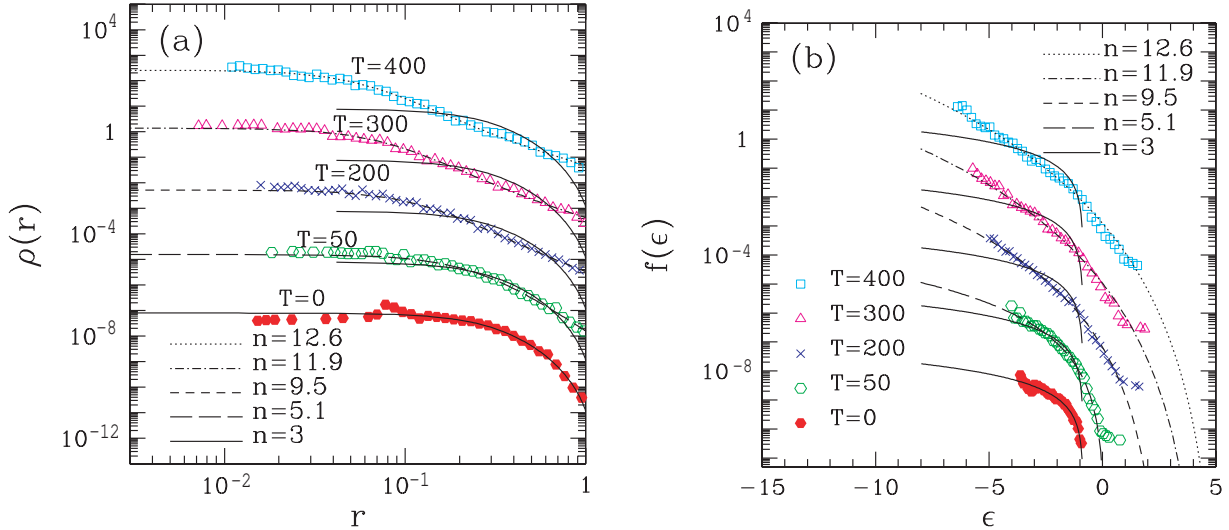


Fig. 4.2. Results from simulation run A, (a) Snapshots of density profile  $\rho(r)$ , (b) Snapshots of one-particle distribution function  $f(\epsilon)$ .

indicate the fitting results to the stellar polytrope by varying the polytrope index  $n$ . Note that the number of fitting parameters just reduces to one, i.e., the polytrope index, since the total energy is well-conserved in the present situation. Fig. 4.2 shows that while the system gradually deviates from the initial polytropic state, the transient state still follows a sequence of stellar polytropes. The fitting results are remarkably good until the time exceeds  $T = 400$ , corresponding to  $15 t_{\text{rel}}$ . Afterwards, the system enters the gravothermal instability regime and finally undergoes the core-collapse.

Now, focus on the evolutionary track in each simulation run summarized in the energy-radius-density contrast plane (Fig. 4.1), where the filled circle represents the initial stellar polytrope. Interestingly, the density contrast of the transient state in run A initially decreases, but it eventually turns to increase. The turning-point roughly corresponds to the stellar polytrope with index  $n = 5.6$ . Note, however, that the time evolution of polytrope index itself is a monotonically increasing function of time [17]. This is indeed true for the other cases, indicating the Boltzmann H-theorem that any of the self-gravitating systems tends to approach the isothermal state. A typical example is the run C2, which finally reaches the stable isothermal state. However, as already shown in run A, all the systems cannot reach the isothermal state. Fig. 4.1 indicates that no isothermal state is possible for a fixed value  $D > 0.335[6]$ , which can be derived from the peak value of the trajectory. Further, stable stellar polytropes cease to exist at high density contrast  $D > D_{\text{crit}}$ . In fact, our simulations starting from the stellar polytropes finally underwent core-collapse due to the gravothermal catastrophe (runs A, B1 and B2). Though it might not be rigorously correct, the predicted value  $D_{\text{crit}}$  provides a crude approximation to the boundary between the stability and the instability.

Fig. 4.3 plots the snapshots of the distribution function taken from the other runs. The initial density contrast in run B1 (Fig. 4.3(a)) is relatively low ( $D = 110$ ) and thereby the system slowly evolves following a sequence of stellar polytropes. After  $T = 2000 - 74 t_{\text{rel}}$ , the system begins to deviate from the stable equilibrium sequence, leading to the core-collapse. Another noticeable case is the run C1 (Fig. 4.3(b)). The Hernquist model's initial distribution of run C has cuspy density profile,  $\rho(r) \propto 1/r - (r + a)^3$ , which behaves as  $\propto 1/r^4$  at the inner part [37]. The resultant distribution function  $f(\epsilon)$  shows a singular behavior at the negative energy region, which cannot be described by the power-law distribution. Soon after a while, however, the gravothermal expansion [36] takes place and the outer core is eventually formed. Then the system settles into a sequence of stellar polytropes and can be approximately described by the stellar polytrope with index  $n = 20$  for a long time. Thus the stellar polytrope can be regarded as a quasi-attractor and a quasi-equilibrium state.

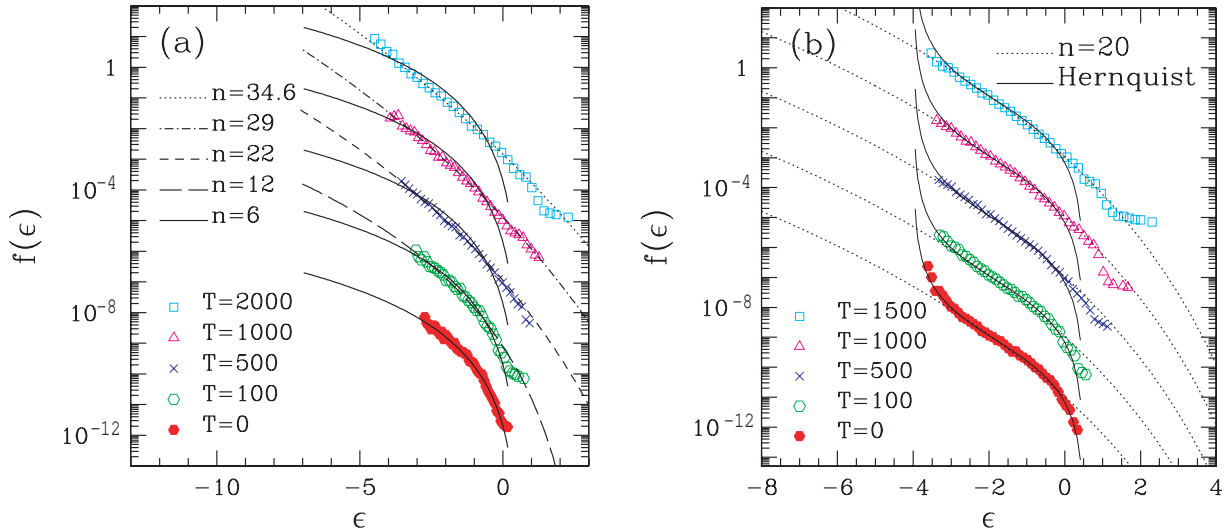


Fig. 4.3. Evolution of one-particle distribution function in other models. (a) run B1. (b) run C1.

## 5 Conclusion and Discussion

In this paper, we discussed the issues on the thermodynamic properties of stellar self-gravitating system arising from the Tully's entropy, with a particular emphasis on the standard framework using the normalized  $q$ -expectation values. It then turns out that the new extremum-entropy state essentially remains unchanged from the previous study and is characterized by the stellar polytrope, although the distribution function shows several distinct properties. Taking these facts carefully, the thermodynamic temperature of the extremum state was identified through the modified Clausius relation and the specific heat was evaluated explicitly. The detailed discussion on the behavior of specific heat finally leads to the conclusion that the onset of gravothermal instability remains unchanged with respects to choice of the statistical average for a system confined in an adiabatic wall (micro-canonical case). As for the system surrounded by a thermal wall (canonical case), although this analysis has been skipped in this article, the stability of the system drastically depends on choice of the statistical average [15, 16]. The existence of these thermodynamic instabilities can also be deduced from the variation of entropy and free-energy rigorously [14, 15, 16]. As a result, above the certain critical values of  $n$  or  $D$ , the thermodynamic instability appears at  $n > 5$  for a system confined in an adiabatic wall.

We have performed a set of numerical simulations of long-term stellar dynamical evolution away from the isothermal state and found that the transient state of the system confined in an adiabatic wall can be remarkably fitted by a sequence of stellar polytropes. This is even true in the case of removing the outer boundary [17]. Therefore, the stellar polytropic distribution can be a quasi-attractor and a quasi-equilibrium state of a self-gravitating system.

## Acknowledgments

We are grateful to P.H. Chavanis for comments and discussions. This work was supported by the Grant-in-Aid from Japan Society of Promotion of Science (No.15540368, No.14740157).

## A Appendix: Evaluation of the relaxation time

Here we shortly evaluate the relaxation time for the self-gravitating many-body systems (2.3). For more precise derivation, consult references [1, 18]. In the kinetic theory, a timescale of relaxation due to 2-body collisions is given by

$$t_{\text{rel}} = \frac{1}{nv}; \quad (\text{A.1})$$

where  $n$  is a mean number density and  $v$  an averaged relative velocity of particles. In order to evaluate amplitude of 2-body collision by mutual gravitational force, we introduce the gravitational radius  $r_g$  as follows,

$$m v^2 \frac{G m^2}{r_g} ! \quad r_g \frac{G m}{v^2} : \quad (A.2)$$

If the impact parameter of the collision between 2 particles of identical mass becomes smaller than the gravitational radius, i.e.  $b < r_g$ , orbits of particles are significantly changed by the close encounter. It follows that the cross section of 2-body collision is given by

$$4 r_g^2 : \quad (A.3)$$

Substituting this estimation and  $n = N = R^3$  into (A.1), we obtain

$$t_{\text{rel}} \frac{v^3 R^3}{4 G^2 m^2 N \ln(R/r_g)} ; \quad (A.4)$$

where  $R$  and  $N$  are the system size and the number of particles, respectively. In the above expression (A.4), we have included the term so called Coulomb logarithm,  $\ln(R/r_g)$ , which appears due to the long-range nature of the interaction [1] and is well-known in the plasma theory. Taking its ratio to the dynamical time  $t_{\text{dyn}} = R/v$ , we obtain

$$t_{\text{rel}} \frac{N}{4 \ln N} t_{\text{dyn}} ; \quad (A.5)$$

where the average velocity is estimated as  $v^2 = G N m / R$  from the virial theorem (2.4).

## References

1. J. Binney, S. Tremaine, *Galactic Dynamics* (Princeton Univ. Press, Princeton, 1987)
2. L. Spitzer, *Dynamical Evolution of Globular Clusters*, (Princeton Univ. Press, Princeton, 1987).
3. R. E. Larson, P. Hut, S. Inagaki, *Ann. Rev. Astron. Astrophys.* 25 (1987) 565.
4. G. Meylan, D. C. Heggie, *Astron. Astrophys. Rev.* 8 (1997) 1.
5. V. A. Antonov, *Vest. Leningrad Univ.*, 7 (1962) 135 (English transl. in IAU Symposium 113, *Dynamics of Globular Clusters*, ed. J. Goodman and P. Hut [Dordrecht: Reidel], pp. 525-540 [1985])
6. D. Lynden-Bell, R. Wood, *Mon. Not. R. Astron. Soc.* 138 (1968) 495.
7. T. Padmanabhan, *Phys. Rep.* 188 (1990) 285.
8. C. T. Sallis, *J. Stat. Phys.* 52 (1988) 479.
9. S. Abe, Y. Okamoto (Eds.), *Nonextensive Statistical Mechanics and Its Applications* (Springer, Berlin, 2001)
10. G. Kaniadakis, M. Lissia, A. Rapisarda (Eds.), *Non-Extensive Thermodynamics and Physical Applications special issue*, *Physica A* 305 (2002)
11. A. R. Plastino, A. Plastino, *Phys. Lett. A* 174 (1993) 384.
12. J.-J. Aly, in *N-body Problems and Gravitational Dynamics*, Proceedings of a meeting held at Aussois-France (21-25 March 1993), (eds.) F. Combes, E. Athanassoula (Publications de l'Observatoire de Paris, Paris, 1993), p. 19.
13. J. A. S. Lima, R. Silva, J. Santos, *Astron. Astrophys.* 396 (2002) 309.
14. A. Taruya, M. Sakagami, *Physica A* 307 (2002) 185.
15. A. Taruya, M. Sakagami, *Physica A* 318 (2003) 387.
16. A. Taruya, M. Sakagami, *Physica A* 322 (2003) 285.
17. A. Taruya, M. Sakagami, *Phys. Rev. Lett.* 90 (2003) 181101.
18. S. Chandrasekhar, *Principles of Stellar Dynamics* (Univ. of Chicago Press, 1942)
19. T. Padmanabhan, *Astrophys. J. Suppl.* 71 (1989) 651.
20. J. K. Katz, *Mon. Not. R. Astron. Soc.* 183 (1978) 765.
21. J. K. Katz, *Mon. Not. R. Astron. Soc.* 189 (1979) 817.
22. *Publ. Astron. Soc. Japan* 32 (1980) 213.
23. I. Hachisu, D. Sugimoto, *Theor. Phys.* 60 (1978) 393.
24. J. Makino, P. Hut, *Astrophys. J.* 383 (1991) 181.
25. P. H. Chavanis, *Astron. Astrophys.* 386 (2002) 732; *ibid.* 401 (2003) 15.
26. P. H. Chavanis, C. Sire, *Phys. Rev. E*, in press (cond-mat/0303088).
27. C. T. Sallis, R. S. Martínez, A. R. Plastino, *Physica A* 261 (1998) 534.
28. S. Martínez, F. Nicolás, F. Pennini, A. R. Plastino, *Physica A* 286 (2000) 489.
29. S. Abe, A. K. Rajagopal, *Phys. Lett. A* 272 (2000) 345; *J. Phys. A* 33 (2000) 8733; *Europhys. Lett.* 52 (2000) 610.
30. S. Chandrasekhar, *Introduction to the Study of Stellar Structure* (New York, Dover, 1939)
31. R. Kippenhahn, A. Weigert, *Stellar Structure and Evolution* (Springer, Berlin, 1990)
32. D. Lynden-Bell, *Physica A* 263 (1999) 293.
33. S. Abe, S. Martínez, F. Pennini, A. R. Plastino, *Phys. Lett. A* 281 (2001) 126.
34. S. Abe, *Physica A* 300 (2001) 417.
35. S. Martínez, F. Pennini, A. R. Plastino, *Physica A* 295 (2001) 416.
36. H. Endoh, T. Fukushige, J. Makino, *Publ. Astron. Soc. Japan* 49 (1997) 345.
37. L. Hernquist, *Astrophys. J.* 356 (1990) 359.

